

Structural basis for disassembly of katanin heterododecamers

Received for publication, December 4, 2017, and in revised form, April 20, 2018. Published, Papers in Press, May 11, 2018, DOI 10.1074/jbc.RA117.001215

Stanley Nithianantham, Francis J. McNally, and Jawdat Al-Bassam¹

From the Department of Molecular Cellular Biology University of California, Davis, California 95616

Edited by Velia M. Fowler

The reorganization of microtubules in mitosis, meiosis, and development requires the microtubule-severing activity of katanin. Katanin is a heterodimer composed of an ATPase associated with diverse cellular activities (AAA) subunit and a regulatory subunit. Microtubule severing requires ATP hydrolysis by katanin's conserved AAA ATPase domains. Whereas other AAA ATPases form stable hexamers, we show that katanin forms only a monomer or dimers of heterodimers in solution. Katanin oligomers consistent with hexamers of heterodimers or heterododecamers were only observed for an ATP hydrolysis-deficient mutant in the presence of ATP. X-ray structures of katanin's AAA ATPase in monomeric nucleotide-free and pseudo-oligomeric ADP-bound states revealed conformational changes in the AAA subdomains that explained the structural basis for the instability of the katanin heterododecamer. We propose that the rapid dissociation of katanin AAA oligomers may lead to an autoinhibited state that prevents inappropriate microtubule severing or that cyclical disassembly into heterodimers may critically contribute to the microtubule-severing mechanism.

Microtubules (MTs)² are dynamic cytoskeleton polymers that are essential force generators that organize the cytoplasm during cell division, development, and morphogenesis. The stability of the MT polymer is mediated by longitudinal and lateral interfaces between $\alpha\beta$ -tubulins polymerized in the MT lattice. Diverse classes of MT regulators promote the polymerization and depolymerization of dynamic MTs by binding $\alpha\beta$ -tubulins at their ends. However, in contrast to these regulators, MT-severing enzymes destabilize MTs by binding along MT lattice

sites to generate several new MTs. The MT-severing proteins include the closely related AAA ATPases katanin, spastin, and fidgetin, which are conserved across protozoa, plants, and metazoans (1). MT-severing enzymes carry out essential MT regulatory functions in many cellular settings in which MT are involved. During mitosis and meiosis, they activate MT disassembly (2, 3). During neuronal development, they are essential to the release of new MTs after nucleation (4), and during cell motility they regulate MT formation in cilia or flagella (5). Defects in human katanin and spastin lead to neurological disorders such as microlissencephaly (6, 7) and hereditary spastic paraplegia (8), respectively.

Katanin, first purified from sea urchin eggs, is composed of a catalytic subunit, termed p60, and a regulatory subunit, termed p80 (9). p60 katanin is composed of an N-terminal microtubule-interacting and trafficking (MIT) domain (10) followed by a 50–70-residue linker and a highly conserved C-terminal AAA ATPase domain. p80 katanin exists in multiple forms, which either include or exclude a large N-terminal β -propeller or WD-40 domain followed by a core conserved 280-residue helical bundle region termed conserved p80 (con80) (2) (Fig. 1A). Both the p60 (MIT and AAA domains) and p80 (con80 with or without WD-40) domains are essential for the MT-severing functions. p60 and p80 katanin form a complex through the con80-MIT domains, the structure of which reveals a helical assembly that is responsible for binding MTs and recruiting MT regulatory factors to sites of MT lattice deformation (2). p60 and p80 katanin co-purify from many cell types (9, 11), and p60 and p80 mutants have identical phenotypes in many organisms (5, 12), indicating that a complex of p60 and p80 is the relevant physiological complex.

Most AAA ATPases are thought to act as hexameric ring complexes. For example, *N*-ethylmaleimide-sensitive fusion (NSF) is greater than 90% hexameric in solution throughout a concentration range of 0.2 to 10 μ M in ATP (13). X-ray or cryo-EM structures of several other WT AAA ATPases have revealed open or closed hexameric rings (14–16). In contrast, members of one subfamily of AAA ATPases are reported to be predominantly monomeric or dimeric in solution. This subfamily includes the MT-severing proteins katanin, spastin, and fidgetin, as well as Vps4 and MSP1, which disassemble non-tubulin substrates (17–21). The WT form of each of these ATPases has most often been shown to be monomeric in solution at low concentrations. In contrast, each of these proteins has been reported to form a stable hexamer at low concentration when ATP hydrolysis is blocked by the mutation of a con-

This work was supported by National Institutes of Health Grants GM110283 (to J. A.-B.) and GM079421 (to F. J. M.). The authors declare that they have no conflicts of interest with the contents of this article. The content is solely the responsibility of the authors and does not necessarily represent the official views of the National Institutes of Health.

This article contains Figs. S1–S8

The atomic coordinates and structure factors (codes 6B5C and 6B5D) have been deposited in the Protein Data Bank (<http://www.pdb.org/>).

¹ To whom correspondence should be addressed. E-mail: jawdat@ucdavis.edu.

² The abbreviations used are: MT, microtubule; MIT, microtubule-interacting and trafficking; VPS4, vacuolar protein sorting-associated protein 4; con80, conserved p80; NSF, *N*-ethylmaleimide-sensitive fusion; SEC, size-exclusion chromatography; SEC-MALS, SEC-coupled multiangle light scattering; AMPPNP, 5'-adenylyl- β , γ -imidodiphosphate; SAD, single-wavelength anomalous dispersion; NBD, nucleotide-binding domain; HBD, 4-helix bundle domain; N-Hlx, N-terminal helix; C-Hlx, C-terminal helix; RMSD, root-mean-square deviation; TEV, tobacco etch virus; GST, glutathione *S*-transferase; PDB, Protein Data Bank.

served Glu (E) in the Walker B motif to Gln (Q) (17–21). Structural studies have revealed that the ATP hydrolysis–deficient Walker B mutant of p60 katanin can form a right-handed hexameric spiral with all six protomers bound by ATP or a closed hexameric ring with five ATP-bound protomers and one nucleotide-free protomer (22). However, earlier fluorescence resonance energy transfer (FRET) experiments indicate that oligomers of WT p60 katanin could be detected only in the presence of both a microtubule substrate and a nonhydrolyzable ATP analog (19). Thus, the structural basis for katanin's disinclination to form hexamers in the absence of a microtubule has remained unclear.

Here, we reconstituted katanin complexes of full-length p60 with core con80 domains using the *Caenorhabditis elegans* MEI-1/MEI-2 and human KATNAL1/KATNB1 forms. We show that p60/p80 is a heterodimer or heterotetramer with a poor capacity for oligomerization into oligomers, most consistent with heterododecamers. The crystal structures for katanin's AAA ATPase in the ADP-bound and nucleotide-free states reveal a substantial conformational transition that could explain katanin's poor propensity for oligomerization.

Results

Catalytically active p60/p80 katanin is composed predominantly of heterodimers or heterotetramers in solution

To examine the oligomerization properties of p60/p80 katanin, we first purified complexes of full-length *C. elegans* MEI-1 with full-length MEI-2 (termed MEI-1/MEI-2), and full-length human KATNAL1 with the con80 domain (residues 411–655) of human KATNB1 (termed KATNAL1/B1-con80) (Figs. 1A and S1, A and B). MEI-1 and KATNAL1 are 51.7- and 55.4-kDa proteins, respectively, whereas MEI-2 and KATNB1-con80 are 31.5- and 26.7-kDa proteins, respectively. Thus, isolated heterodimers of MEI-1/MEI-2 or KATNAL1/B1-con80 are roughly 83 kDa in mass. KATNAL1/B1-con80 complexes were studied using a Superose 6 size-exclusion chromatography (SEC) column at katanin concentrations ranging from 5 to 50 μM in the presence of 1 mM ATP (Figs. 1, B and D, and S2A). Two overlapping peaks eluted earlier at higher concentrations, indicating a concentration-dependent increase in Stokes radius as reported previously for MEI-1/MEI-2 complexes (23). SDS-PAGE of the peak fractions indicated that the subunit masses and the stoichiometry of KATNAL1 to B1-con80 were the same in all the peak fractions at all concentrations (Fig. 1, D and E, and S2A). To test whether this increase in Stokes radius was because of an increase in mass due to oligomerization of heterodimers, 10–50 μM KATNAL1/B1-con80 complexes were analyzed by SEC-coupled multiangle light scattering (SEC-MALS) in the presence of 1 mM ATP using a Superdex 200 column (Fig. 1C and Table 1). The two peaks of katanin complexes were more clearly resolved using a Superdex 200 SEC column. SEC-MALS measurements indicated a mass for the faster eluting complex that was most consistent with a dimer of heterodimers (heterotetramer) and a mass for the slower eluting complex that was most consistent with a heterodimer (Fig. 1C). Strikingly, the SEC-MALS-measured masses did not change in the range of 10 to 50 μM katanin

(Table 1) even though the Stokes radii increased in this concentration range (Fig. 1, B and C). *C. elegans* MEI-1/MEI-2 eluted as a single peak in the absence of ATP (Fig. S1A). SDS-PAGE and quantitation of MEI-1 to MEI-2 molar ratios indicated a 1:1 molar ratio similar to human KATNAL1/B1-con80 complexes (Fig. S1D). MALS measurements of MEI-1/MEI-2 indicated a mass intermediate between that of a dimer of heterodimers and that of a trimer of heterodimers (MEI-1/MEI-2 heterodimer, 83 kDa; and SEC-MALS-measured mass, 216 kDa) (Fig. S1, C–E and Table 1), suggesting a possible equilibrium but no assembly into a hexamer of heterodimers. Our SEC-MALS results indicate that WT KATNAL1/B1-con80 does not assemble beyond dimers of heterodimers at concentrations up to 50 μM . For WT KATNAL1/B1-con80, masses were identical in the absence (dimers of heterodimers measured mass, 164–169 kDa; predicted mass, 164.2 kDa) (Figs. 1F and S2B) or in the presence (Figs. 1G and S2B and Table 1) of ATP. Previous studies of katanin (19, 22) and spastin (18) indicate that a Glu \rightarrow Gln mutation in the Walker B motif stabilized a hexameric assembly only in the presence of ATP. Indeed, an E308Q variant of KATNAL1/B1-con80 had a mass most consistent with a heterododecamer or hexamer of heterodimers (measured mass, 505 kDa; and predicted mass, 492 kDa) only in the presence of ATP (Fig. 1G and Table 1). In the absence of ATP, KATNAL1 (E308Q)/B1-con80 eluted as two peaks with masses consistent with heterodimer and dimer of heterodimers (heterotetramer), similar to WT KATNAL1/B1-con80 with or without ATP. Strikingly, the Stokes radius of a KATNAL1 (E308Q)/B1-con80 hexamer of heterodimers (heterododecamer) was nearly identical to that of a WT dimer of heterodimers (heterotetramer) at the same concentration, suggesting that the dimer of heterodimers has an elongated conformation (Fig. 1G). SDS-PAGE and quantitation of molar ratios for KATNAL1 WT or E308Q compared with KATNB1-con80 show that they are present at 1:1 molar stoichiometry and that there are no differences in subunit compositions in the different states (Fig. 1E and Fig. S2). Previous work estimates the *in vivo* concentration of katanin at 20–50 nM (11). Our results thus indicate that WT katanin does not form hexamers of heterodimers (heterododecamers) at concentrations 1000 times higher than physiological concentrations and suggest that, in solution, WT katanin is in an autoinhibited state in the presence or absence of nucleotide. Furthermore, ATP is required for the oligomerization of KATNAL1 (E308Q)/B1-con80, suggesting that dissociation of the nucleotide returns katanin to its autoinhibited state (Fig. 1, G and H).

Crystal structure of MEI-1's AAA ATPase in the ADP-bound state reveals a pseudo-hexameric left-handed spiral assembly

To understand the structural basis for nucleotide-driven katanin oligomerization, we aimed to determine the crystal structure of katanin with the nonhydrolyzable ATP analog AMPNP. Although we crystallized the full-length *C. elegans* p60 katanin in complex with the con80 domain of p80, MEI-1/MEI-2 crystals contained only the AAA ATPase domains and bound ADP molecules. The MIT/Con80 domains degraded during crystallization, likely because of the prolonged incubation (14 days) required for crystallization (Fig. S2F). The AMPNP presumably either hydrolyzed during crystallization or

Katanin nucleotide-free state reveals disassembly mechanism

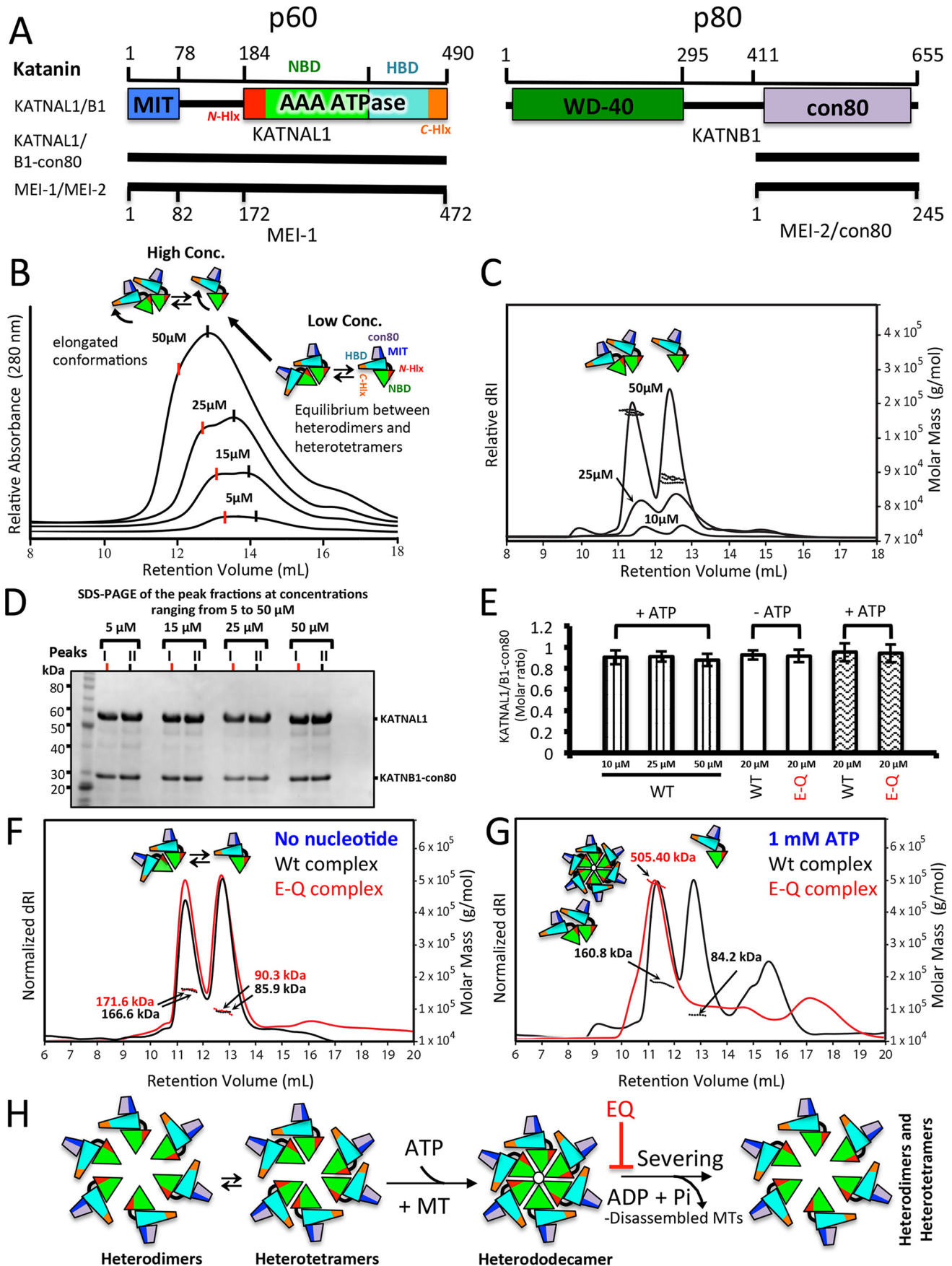


Table 1
Oligomeric assembly activity of katanin

Protein	Conc.	Nucleotide	Hetero-dimer ^{a,b}	Heterotetramer ^{c,d}	Heterododecamer ^e	Subunit molar ratio (SDS-PAGE)
	μM	1 mM	kDa	kDa	kDa	
WT KATNAL1/B1-con80	10	ATP	93.81 ± 5.26	166.51 ± 6.00		0.903 ± 0.067
WT KATNAL1/B1-con80	25	ATP	98.77 ± 4.82	164.60 ± 5.40		0.910 ± 0.047
WT KATNAL1/B1-con80	50	ATP	87.88 ± 3.20	169.01 ± 2.20		0.879 ± 0.056
WT KATNAL1/B1-con80	20	ATP	84.23 ± 6.70	160.80 ± 4.40		0.952 ± 0.085
WT KATNAL1/B1-con80	20		85.98 ± 7.80	166.60 ± 3.60		0.925 ± 0.043
KATNAL1 (E308Q)/B1-con80	25	ATP			505.40 ± 4.02	0.941 ± 0.085
KATNAL1 (E308Q)/B1-con80	25		90.30 ± 1.21	171.60 ± 4.12		0.916 ± 0.058
WT MEI-1/MEI-2	50			216.50 ± 7.10 ^{d,f}		0.923 ± 0.091

^a Calculated mass for KATNAL1/B1-con80 heterodimer: 82.1 kDa (55.4 + 26.7 = 82.1 kDa).

^b Calculated mass for a MEI-1/MEI-2 heterodimer: 83.2 kDa (51.7 + 31.5 = 83.2 kDa).

^c Calculated mass for a heterotetramer (dimer of KATNAL1/B1-con80 heterodimers): 164.2 kDa.

^d Calculated mass for a heterotetramer (dimer of MEI-1/MEI-2 heterodimers): 166.4 kDa.

^e Calculated mass for a heterododecamer (hexamer of KATNAL1/B1-con80 heterodimers): 492.6 kDa.

^f Calculated mass for a heterohexamer (trimer of MEI-1/MEI-2 heterodimers): 249.6 kDa.

never exchanged with nucleotide bound during bacterial expression. Crystals of *C. elegans* MEI-1/MEI-2 formed in the presence of ADP in the space group $P6_5$ and diffracted to 3.1-Å resolution. Phase information was determined by single-wavelength anomalous dispersion (SAD) using selenomethionine-substituted protein (see “Experimental procedures”). The refined 3.1-Å structure includes only part of the AAA-MIT linker region (residues 164–171) and the MEI-1 AAA domain starting at residue 172 and extending to residue 468 (Fig. 2, A and B, and Table 2) in which three flexible loops are disordered (see “Experimental procedures”). The structure reveals an AAA ATPase fold with ADP (Fig. 2B) that is similar to the recently reported X-ray structure of the E to Q ATP hydrolysis deficient mutant of sulfate-bound MEI-1 AAA (22). Briefly, as with all AAA structures, MEI-1 AAA consists of a larger nucleotide-binding domain (NBD) and a smaller 4-helix bundle domain (HBD). The NBD is in an α/β Rossman fold consisting of a 5-stranded parallel β -sheet ($\beta 1$ – $\beta 5$) sandwiched between nine α -helices ($\alpha 2$ – $\alpha 10$). The NBD cradles an ADP molecule via Walker A and Walker B motifs (Fig. 2, E and F). The HBD is composed of a central α -helix bound orthogonally by four antiparallel helices ($\alpha 11$ – $\alpha 13$ and $\alpha 16$) with its sensor II motif. Two additional short helices ($\alpha 14$ – $\alpha 15$) were inserted between $\alpha 13$ and $\alpha 16$. This insertion is replaced by the β -domain in the Vps4 AAA ATPase (21). The MEI-1 AAA structure reveals two highly conserved katanin expansion AAA ATPase segments as seen previously (22), which we term the N-terminal ($\alpha 1$, N-Hlx) and C-terminal ($\alpha 17$, C-Hlx) helices, respectively (Figs. 2, A and B, and S3). The N-Hlx consists of a single-turn helix bound along one side of the NBD followed by a linker and a three-turn helix bound along the opposing face of the NBD (Fig. 2B). The C-Hlx stabilizes the NBD and HBD junction, connected by a

short loop that we term the hinge. Like the Glu → Gln mutant structure (22), our WT MEI-1 AAA structure reveals the conformation of the AAA subdomains in a pseudo-oligomeric assembly state. In this structure, the protomers are arranged along a pseudo-hexameric staircase-like screw axis with one subunit in the asymmetric unit (Fig. 2C). The projection of this structure parallel to this crystallographic screw axis reveals a pseudo-hexameric left-handed spiral assembly with a 14-Å translation between two adjacent subunits (Fig. S4, A and B). In this conformation, the NBD and ADP of one AAA subunit is bound by an HBD via the sensor II motif with a 1112-Å² buried surface/monomer that might reflect the functional contacts of a physiologically relevant oligomer (Fig. 2, C, E, and F). The expansion N-Hlx and the C-Hlx line opposite sides of this left-handed katanin spiral. ADP was clearly defined in our MEI-1 structure, suggesting a possible relationship between ADP binding and the left-handed spiral assembly. Alternatively, this ADP-bound structure could represent a monomer that is competent to assemble into a right-handed hexameric spiral or closed ring (22). Clearly, neither a continuous spiral nor a hexameric ring formed in our SEC-MALS experiments on WT KATNAL1/B1-con80, and therefore we sought a possible mechanism to prevent assembly in solution.

Crystal structure of KATNAL1's AAA ATPase in the nucleotide-free state reveals a monomer

We also attempted to determine the structure of human KATNAL1 (E308Q)/B1-con80, and crystals grew in the space group $P2_12_12_1$. We observed the degradation of the MIT/con80 domains during crystallization similar to MEI-1/MEI-2, likely because of the prolonged incubation time required for crystals to form. We determined the X-ray structure of the KATNAL1

Figure 1. Domain structures and biochemical characterization of katanins. A, schematic representation of *Homo sapiens* katanin, a heterodimer of p60 and p80 proteins (KATNAL1/KATNB1) consisting of MIT (blue), AAA ATPase (red, N-Hlx; light green, NBD; cyan, 4-helix-bundle domain or HBD; orange, C-Hlx), β -propeller or WD-40 (green), and conserved p80 or con-80 (light purple) domains, respectively. The KATNAL1/B1-con80 and *C. elegans* MEI-1/MEI-2 constructs are shown below. B, SEC-based analysis of WT KATNAL1/B1-con80 at concentrations ranging from 5 to 50 μM in the presence of 1 mM ATP using size-exclusion chromatography (Superose 6 column). Note that the complex migrates more slowly at lower concentrations, suggesting that KATNAL1/B1-con80 is in equilibrium. C, SEC-MALS of WT KATNAL1/B1-con80 at the same concentrations in the presence of 1 mM ATP using a Superdex 200 column shows monomer to dimers of heterodimers (heterodimers and heterotetramers), revealing that the complex is in equilibrium. D, SDS-PAGE of the peak fractions (red and black marks) of WT KATNAL1/B1-con80 complexes as shown in B at concentrations ranging from 5 to 50 μM in the presence of 1 mM ATP, revealing that WT KATNAL1/B1-con80 complex does not degrade during the SEC runs. E, quantification of KATNAL1 or KATNAL1 (E308Q) to KATNB1-con80 molar ratios measured from SDS-PAGE shown in Fig. S2, A and B. F, SEC-MALS of WT (black) and E308Q mutant (red) of KATNAL1/B1-con80 reveals that the complexes are in a heterodimer–heterotetramer equilibrium in the absence of 1 mM ATP. G, SEC-MALS curves reveal that KATNAL1 (E308Q)/B1-con80 (red) forms a heterododecameric assembly in the presence of 1 mM ATP but only a heterotetrameric assembly with WT KATNAL1/B1-con80 (black). H, schematic reaction scheme of katanin p60/p80 oligomerization and the role of ATP binding and hydrolysis in this process.

Katanin nucleotide-free state reveals disassembly mechanism

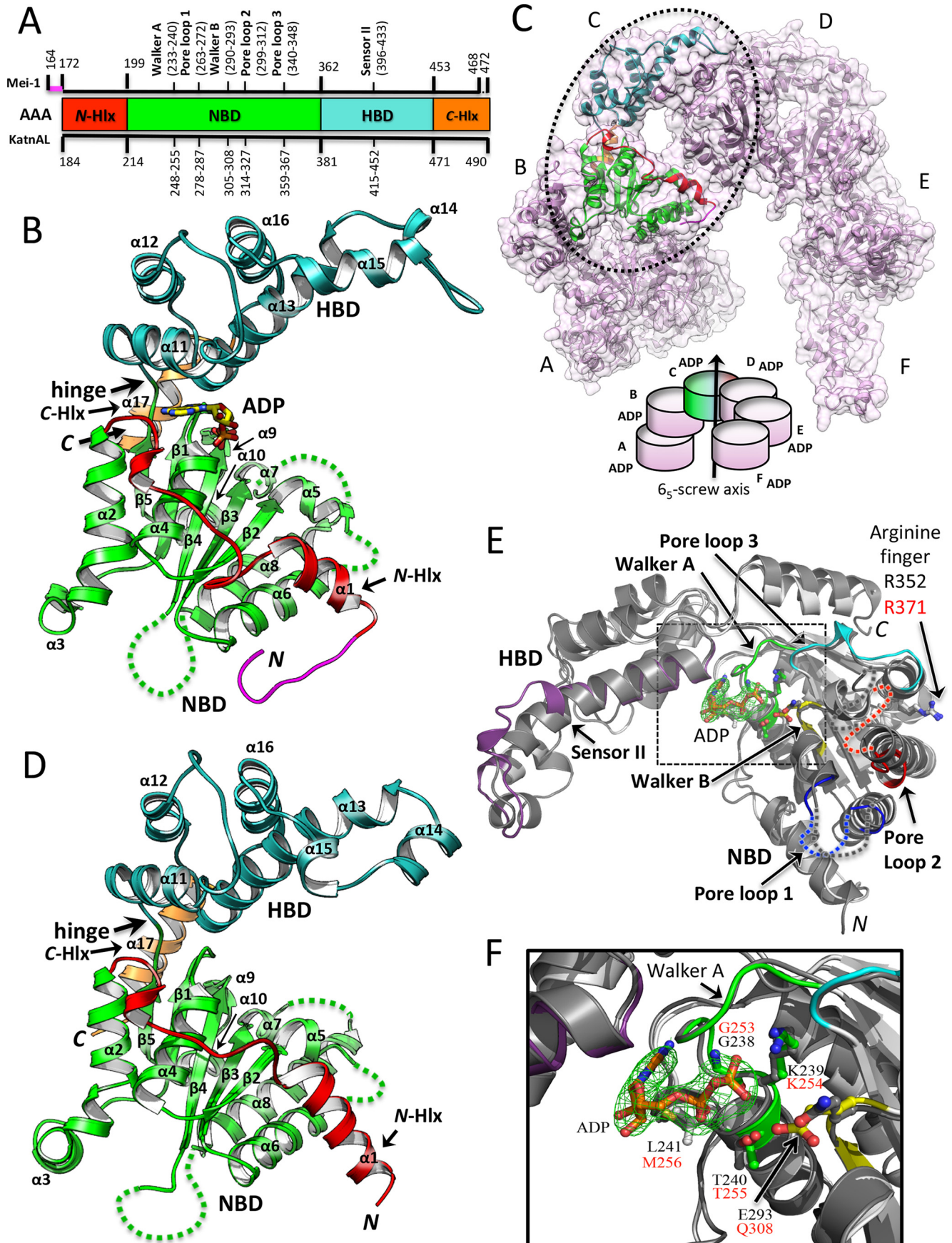


Table 2**Crystallographic statistics**

Numbers in parentheses represent the highest resolution shell.

Statistics	KATNAL1 (E308Q) AAA	KATNAL1 (E308Q) AAA gold derivative (Peak)	MEI-1 AAA (SeMet peak)
Data collection			
Resolution range (Å)	61.19–2.40 (2.53–2.40)	60.88–3.90 (4.11–3.90)	85.59–3.10 (3.27–3.10)
Space group	$P2_1 2_1 2_1$	$P2_1 2_1 2_1$	$P6_5$
Wavelength (Å)	0.9792	1.0388	0.9791
Unit cell (Å): a, b, c	40.10, 61.19, 117.62	40.30, 60.88, 118.70	98.83, 98.83, 75.08
Total number of observed reflections	7,3593 (7317)	1,1699 (1763)	3,7571 (5592)
Unique reflections	1,1932 (1713)	2897 (414)	7653 (1118)
Average mosaicity	0.71	0.45	0.85
Anomalous Multiplicity		2.3 (2.3)	2.4 (2.4)
Multiplicity	6.2 (4.3)	4.0 (4.3)	4.9 (5.0)
Anomalous completeness (%)		92.9 (95.6)	94.7 (94.6)
Completeness (%)	99.9 (99.4)	98.8 (99.2)	99.6 (100.0)
$\langle I/\sigma(I) \rangle$	10.4 (2.1)	4.7 (3.0)	13.0 (2.4)
R_{merge}^a	0.094 (0.569)	0.18 (0.42)	0.076 (0.624)
Structure refinement			
R_{work}	0.22 (0.28)		0.21 (0.24)
R_{free}	0.25 (0.32)		0.26 (0.35)
Molecules/asymmetric unit	1		1
Number of atoms	2385		2229
Protein atoms	2319		2202
Ligand atoms	13		27
RMS bond lengths (Å)	0.002		0.003
RMS bond angles (°)	0.51		0.70
Ramachandran favored (%)	97.5		94.2
Ramachandran allowed (%)	2.1		5.1
Ramachandran outliers (%)	0.4		0.7
Clash score	5.0		8.0
Mean B -values (Å ²)			
Overall	54.33		99.20
Macromolecules	54.27		99.36
Ligands	78.13		86.36
Water	51.17		

$$^a R_{\text{merge}} = \frac{\sum_{hkl} \sum_i |I_i(hkl) - I_{av}(hkl)|}{\sum_{hkl} \sum_i I_i(hkl)}$$

(E308Q) AAA ATPase using partial molecular replacement phases with the NBD domain of the MEI-1 AAA structure combined with SAD phases from a gold derivative. The refined 2.4-Å X-ray structure reveals a single AAA ATPase subunit in the asymmetric unit (Figs. 2D and S4C and Table 2), suggesting that the katanin AAA ATPase is in a monomeric state without nucleotide bound in the NBD pocket. In this structure, katanin does not form any typical AAA ATPase oligomeric interfaces with neighboring AAA subunits, and unlike either MEI-1 AAA structure, this structure is not in a spiral-like conformation (Fig. S4C). The KATNAL1 (E308Q) AAA structure shows ordered density from residues 184 to 490 ($\alpha 1$ – $\alpha 17$ and $\beta 1$ – $\beta 5$) including the last three or four conserved residues of C-terminal $\alpha 17$ (C-Hlx), which were absent from either MEI-1 AAA structure (Ref. 22 and Figs. 2D and S3). The structure shows elements in the nucleotide-binding pocket including the Walker A and Walker B motifs in a conformation similar to those in the MEI-1 AAA structure; however, density for any nucleotide, or any potential mimic, is completely absent in this structure (Figs. 2, E and F, and S3, and S6). The absence of nucleotide or any potential mimic molecule (sulfate or chloride ion) in the crys-

tals reveals that KATNAL1 (E308Q) AAA is a monomer (Fig. 1D and Table 1). Thus, this structure likely represents the auto-inhibited state of the katanin AAA domain.

The differences between our ADP-bound MEI-1 structure and our nucleotide-free KATNAL1 structure might be because of sequence divergence between human KATNAL1 and *C. elegans* MEI-1 (47% identity and 85% similarity) or might reflect differences between the ADP-bound and nucleotide-free states during an ATP hydrolysis cycle. The suggestion that the left-handed spiral assembly of katanin reflects a transient ADP-bound intermediate and our monomeric structure represents a transient nucleotide-free state might appear to be inconsistent with the earlier X-ray structures of MEI-1 AAA (22) and spastin (18, 24). Katanin and spastin AAA domains crystallized in a left-handed spiral arrangement with no nucleotide bound. Therefore, we analyzed the density content in the nucleotide pockets from the deposited maps for two spastin AAA and MEI-1 (Glu \rightarrow Gln) structures to our MEI-1 AAA-ADP structure (18, 22, 24) (Fig. S6). Density maps of the ATP nucleotide-binding pockets revealed the presence of chloride ion or sulfate molecules in the published katanin and spastin structures. The

Figure 2. X-ray structures of ADP-bound MEI-1 AAA and monomeric nucleotide-free KATNAL1 (E308Q) AAA. A, domain diagrams and numbering schemes for katanin AAA (color-coded according to the X-ray structures). Conserved motifs are shown in the schemes. B, ribbon diagram of MEI-1 AAA structure in the ADP state: N-terminal linker, magenta; N-Hlx, red; NBD, light green; HBD, cyan; C-Hlx, orange. The ADP is shown as a stick representation. C, the projection of MEI-1 AAA structure parallel to crystallographic δ_5 -screw axis shows a pseudo-hexameric left-handed spiral assembly. It is shown as a ribbon diagram (light pink) with a transparent surface representation background. One of the subunits is colored according to the crystal structure. D, ribbon representation of KATNAL1 (E308Q) AAA in a nucleotide-free monomeric state. Domains are colored similar to the MEI-1 AAA structure. E, overlay of MEI-1 AAA (pore loops 1–3, sensor II, Walker A, Walker B, and backbone are colored in blue, red, cyan, purple, light green, yellow, and dark gray, respectively), with the bound ADP molecule along with its interacting residues shown in a ball-and-stick representation, and KATNAL1 (E308Q) AAA (white). The initial difference Fourier electron density contoured at 3σ for ADP is shown in green. F, close-up view (enlarged) of the ADP-binding pocket including the motifs shown in similar conformation as described in E.

Katanin nucleotide-free state reveals disassembly mechanism

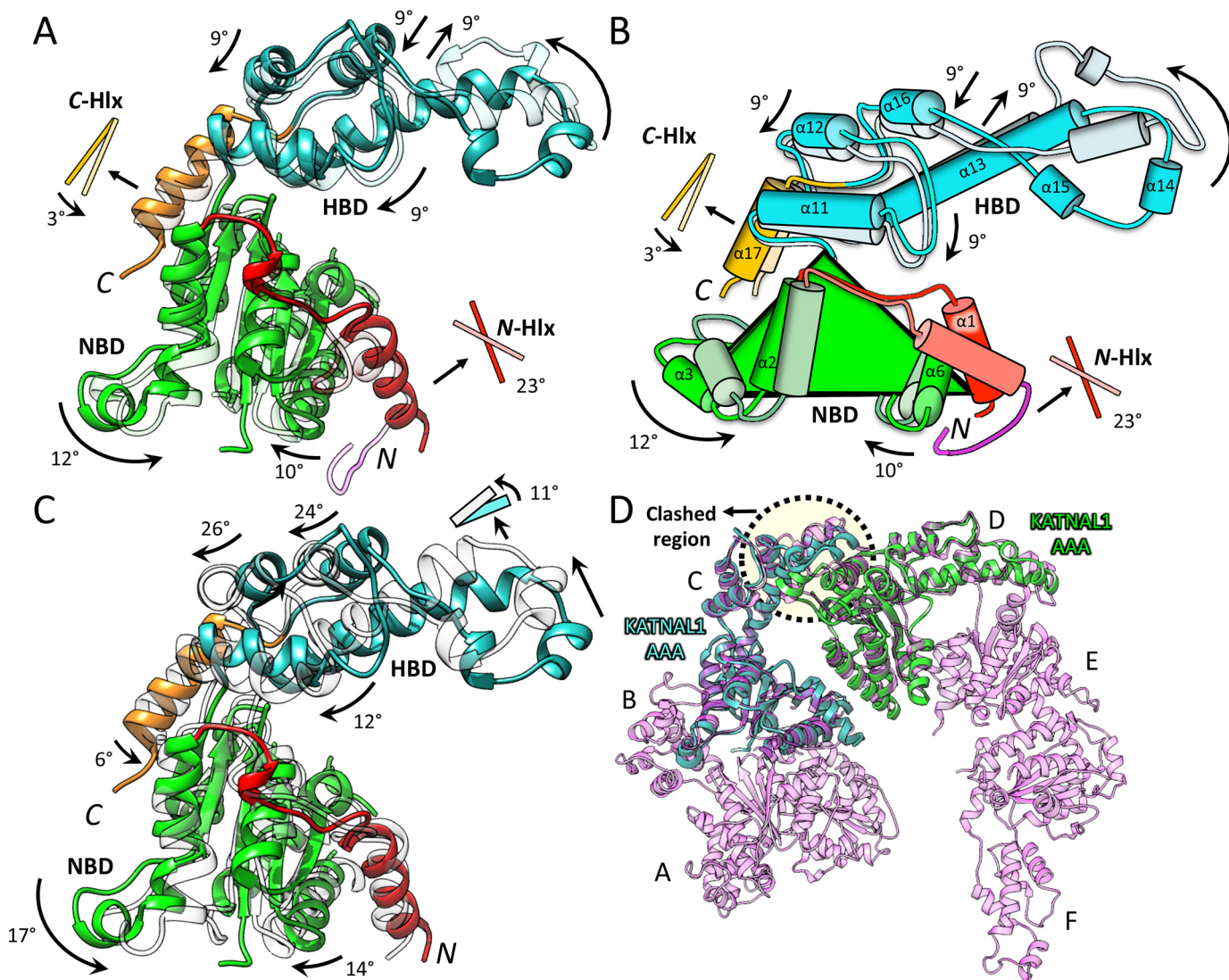


Figure 3. Structural comparison of katanin AAA subdomains and elements in monomeric and pseudo-oligomeric states. Arrows indicate the direction of rotational movements in all of the panels. *A*, superimposition of KATNAL1 (E308Q) AAA (color-coded according to the structure) onto ADP-bound MEI-1 AAA (faded colors) structure. *B*, schematic representation of the MEI-1 AAA (dark colors) overlaid onto the KATNAL1 (E308Q) AAA (faded colors) as described in *A*. *C*, superimposition of nucleotide-free state KATNAL1 (E308Q) AAA (color-coded) onto ATP-state KATNAL1 AAA structures. The ATP model was generated based on MEI-1 hexameric right-handed spiral assembly structure (22). *D*, superimposition of nucleotide-free KATNAL1 (E308Q) AAA structures (cyan and green) onto two adjacent protomers in ADP-bound MEI-1 AAA pseudo-hexameric left-handed spiral (light pink) with the backbones shown as ribbon diagrams. The clashed region (highlighted by dotted-line yellow background circle) shows that the conformation of KATNAL1 (E308Q) AAA is not compatible with pseudo-hexameric left-handed spiral assembly and it is in an auto-inhibited state.

β -phosphate of ADP in our MEI-1 structure resides in a position similar to the anion in the other structures (Fig. S6, A–D). Thus, we suggest that these molecules may mimic ADP nucleotide-bound states in the previously published katanin and spastin structures, which all form spiral assemblies. We further suggest that only our KATNAL1 (E308Q) AAA structure is in a true monomeric, nucleotide-free conformation. The human KATNAL1 autoinhibited state might be more stable compared with that of MEI-1 or spastin.

Structural comparisons of katanin's AAA ATPase in the ATP, ADP, and nucleotide-free states reveal a conformational transition that inhibits oligomerization

We compared the MEI-1 AAA ATPase structure in its pseudo-hexameric ADP state to the KATNAL1 (E308Q) AAA structure in its monomeric nucleotide-free state by superim-

posing the AAA domains in the two structures. The AAA ATPase structures show a root-mean-square deviation (RMSD) of 1.50 Å ($C\alpha$ positions) (Fig. 3, A and B). The comparison reveals that the NBD fold becomes decompressed because of conformational changes in the N-Hlx and C-Hlx and a refolding of the HBD domain. In the monomeric structure, the C-Hlx rotates 3°, whereas the second segment of the N-Hlx rotates 23° azimuthally (Fig. 3, A and B). The detailed interactions of the N-Hlx and C-Hlx with the NBD are shown in Fig. S5. The HBD undergoes a significant refolding rearrangement in which sensor II elements are reorganized. In the ADP state, the central helix, $\alpha 13$, in the HBD is flanked by a parallel helix, $\alpha 15$, near the tip of the HBD. However, in the monomeric structure, the central helix in the HBD ($\alpha 13$) lengthens by two turns through refolding, and the parallel helix (originally $\alpha 15$) refolds into two 2-turn helices ($\alpha 15$ and $\alpha 14$), which are oriented in

nearly orthogonal orientation to $\alpha 13$. The HBD ($\alpha 11$ – $\alpha 13$ and $\alpha 16$) rotates 9° closer to the NBD. In this conformation, the HBD fold reorganizes and changes orientation, leading to clockwise subdomain rotation ($\alpha 15$ and $\alpha 14$) (Fig. 3, A and B). The NBD in the monomeric structure shows decompression-like transitions compared with its fold in the pseudo-oligomeric structure, including a 12° rotation of the $\alpha 2$ – $\alpha 3$ helix-loop-helix elements, and a 10° $\alpha 6$ rotation. These NBD transitions involve elements that mediate NBD–HBD interfaces in the pseudo-oligomeric state.

To find out the difference between the ATP and nucleotide-free states, we built a homology model of a KATNAL1 AAA–ATP state structure based on the previously published cryo-EM structure of the MEI-1 Glu \rightarrow Gln mutant in an ATP-bound hexameric state (22). We calculated those helical movements mentioned previously by superimposing the two structures (RMSD 2.43 Å; C α positions), revealing that the rotational motions of these helices in the ATP state are amplified into slightly larger motions. The rotation angles are indicated in Fig. 3C. These findings suggest that the conformation of katanin is strictly dependent on ATP or ADP binding. The overlay of the KATNAL1 (E308Q) AAA monomeric X-ray structure onto the MEI-1 AAA spiral assembly reveals that the HBD in the KATNAL1 (E308Q) AAA structure is not compatible with its docked state onto the NBD in the MEI-1 AAA structure. The conformation of the HBD in the monomeric state likely inhibits AAA pseudo-oligomeric assembly by interfering with its NBD interface (Figs. 3D and 4). The monomeric nucleotide-free conformation is also incompatible with the hexameric right-handed spiral assembly of MEI-1 EQ AAA, the hexameric closed-ring assembly of MEI-1 EQ AAA, and the hexameric ring assembly of Vps4 in the substrate-bound state (22, 25) (Fig. 5). The RMSD values between KATNAL1 (E308Q) AAA and various katanin AAA ATPase ortholog structures are given in Table 3, revealing that ADP-state MEI-1 AAA and nucleotide-free-state KATNAL1 (E308Q) AAA structures are in different conformations (Fig. 6). The nucleotide-free structure of KATNAL1 thus might reveal the structural basis for autoinhibition.

Mapping *mei-1* mutations onto the full p60 katanin structural model

Using the sequenced *mei-1* loci (26), we mapped the locations of these point mutations onto the full-length p60 structure, including both AAA ATPase and MIT domains. The MIT domain of MEI-1 was modeled based on the recent crystal structure of *Mus musculus* p60N/p80C katanin complex (2). The map of the *mei-1* mutations is shown in Fig. 7, suggesting that the majority of the residues fall in the NBD. These mutations likely lead to its misfolding or interfere in its ability to bind ATP. Three of these *mei-1* mutations (*sb3*, *sb23*, *ct103*) lie at the junction of the NBD and HBD subdomains. One *mei-1* mutation (*ct89*) lies in the HBD tip region, which we hypothesized is important for self-regulated monomer-to-oligomer conformational change. A single *mei-1* mutation (*ct99*) lies in the MIT domain and likely destabilizes the MIT structure and interferes with MT binding. Only a single *mei-1* mutation (*ct84*) is exposed on the surface, suggesting that it may interfere with NBD–NBD assembly as formed in the katanin oligomers.

Discussion

Here, we studied the biochemical and structural mechanisms for assembly and disassembly of katanin oligomers and revealed a role for ATP hydrolysis in this process. Our SEC-MALS analysis clearly demonstrated that human KATNAL1/B1-con80 does not assemble beyond a dimer of heterodimers (heterotrimer), even at concentrations up to $50 \mu\text{M}$. This result is consistent with calculations of native molecular weight for sea urchin p60/p80 katanin (9, 27) and is supported by SEC-MALS and SEC results suggesting that *C. elegans* MEI-1/MEI-2, which we show, is an equilibrium between a dimer and a trimer of heterodimers. Our results are in contrast with analytical ultracentrifugation results indicating that *C. elegans* MEI-1 alone hexamerizes at high concentration (22) and SEC results indicating MEI-1/MEI-2 can form hexamers of heterodimers (22, 23). The *in vivo* concentration of katanin p60/p80 in HeLa cells was estimated to be 20–50 nM using an antibody that cross-reacts with both KATNA1 and KATNAL1 (11). Thus, human katanin's poor propensity for oligomerization may have an important regulatory role in restricting its activities to cellular locations like spindle poles, where it is concentrated and co-localized with positive regulators like ASPM1 (2). Alternatively, the dissociation of katanin heterodimers upon the release of ADP from heterododecamers might be an essential step in the microtubule-severing cycle. A recent model for ESCRT-III disassembly by VPS4 suggests a role for a treadmilling hexameric spiral in which a new ATP-bound VPS4 is added at one end and ATP hydrolysis results in dissociation of a VPS4 at the other end (28). If katanin functioned in a similar way, both the right-handed spiral and closed-ring structures determined by Zehr *et al.* (22) would require complete dissociation of the “oldest” protomer before a new ATP-bound protomer could be added. The nucleotide-free state KATNAL1 AAA structure presented here is incompatible with all the possible oligomeric assemblies such as right-handed hexameric spiral, hexameric ring, and left-handed pseudo-hexameric spiral.

The left-handed ADP-MEI-1 spiral X-ray structure has been discounted previously as a crystal-packing artifact, as it could form endless oligomers, which have not been detected in solution. Our nucleotide-free KATNAL1 AAA monomer X-ray structure would explain how this spiral assembly might be capped and rapidly disassemble upon ADP release. The ATP-bound hexameric ring structures described by Zehr *et al.* (22) were detected only with a specific Glu to Gln mutation, which inactivates ATP hydrolysis. Likewise, further support for the ADP-bound left-handed spiral will require a mutation that stabilizes this transient state.

Using our two experimentally determined X-ray structures, the previously described cryo-EM models for katanin, as well as hexameric Vps4 homology models (Fig. S7), we describe a revised model for katanin MT-based oligomerization and MT severing that includes both the self-inhibited monomeric nucleotide-free and the ADP left-handed spiral states. Our model incorporates the important oligomeric conformational transition described previously by Zehr *et al.* (22) (Figs. 8 and S8). We suggest that p60/p80 katanin heterodimers have a poor propensity for oligomerization because of the self-inhibited

Katanin nucleotide-free state reveals disassembly mechanism

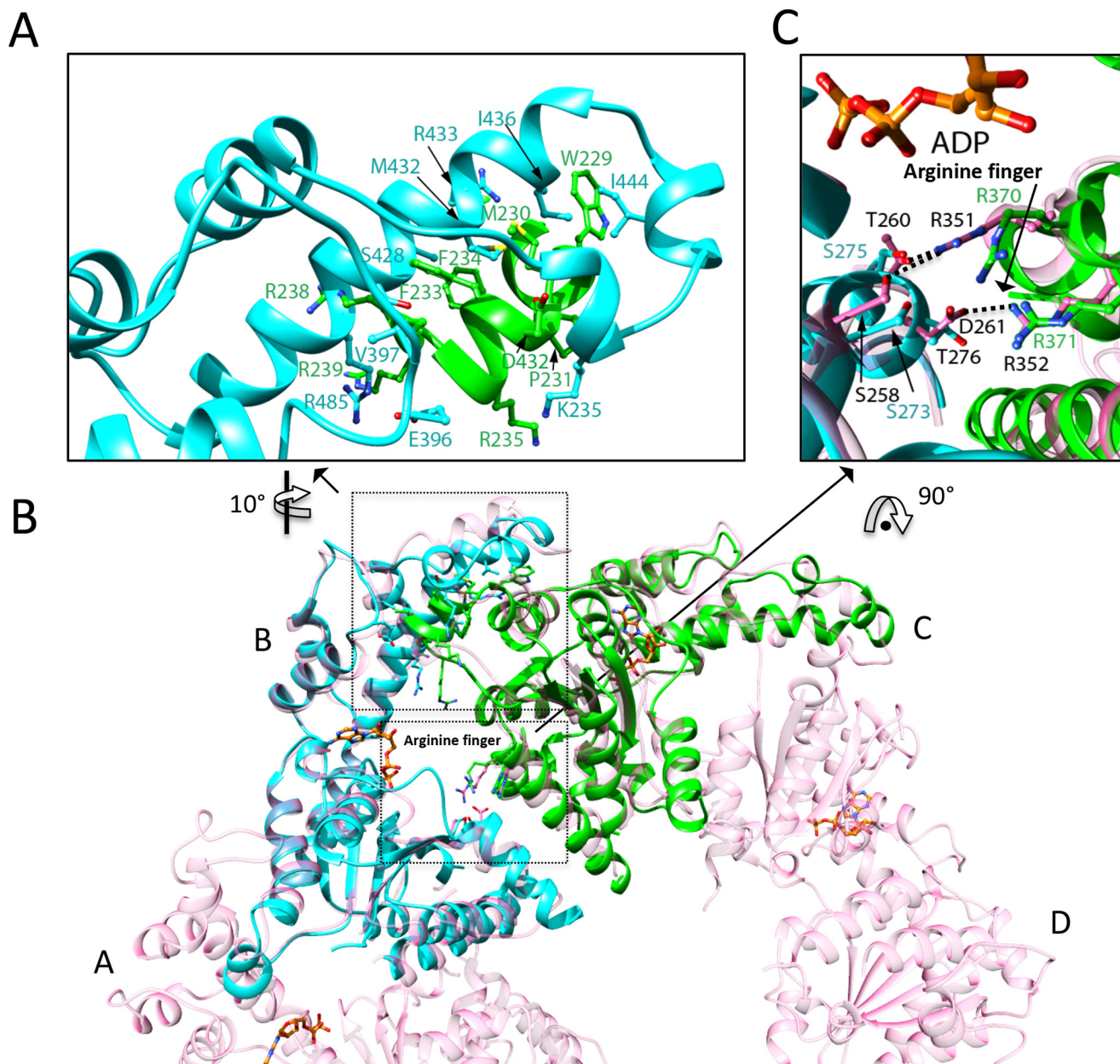


Figure 4. KATNAL1 structure is incompatible with ADP-bound pseudo-hexameric left-handed spiral assembly. *A* and *B*, the clashed region reveals that the KATNAL1 (E308Q) AAA structure is not compatible with pseudo-hexameric assembly when two KATNAL1 (E308Q) AAA structures (cyan and green) are superimposed onto two adjacent protomers in ADP-bound pseudo-hexameric left-handed spiral assembly (light pink). A close-up view of the clashed region is shown in *A*. Note that pseudo-hexameric assembly was removed for clarity. The clashed residues are shown as ball-and-stick models. *C*, close-up view of pseudo-hexameric spiral interface revealing that the left-handed spiral assembly is stabilized by ionic interactions through arginine residues including an arginine finger (R352) in the MEI-1 AAA structure. The KATNAL1 (E308Q) AAA superimposed structures reveal that loss of ionic interactions due to decompression of NBD domain leads to an autoinhibited state.

AAA conformation in our KATNAL1 nucleotide-free structure. Katanin heterodimers likely bind along the MT lattice via the MIT/Con80 interface. These katanin p60/p80 heterodimers would diffuse along MT lattices, bind ATP, and begin to assemble into right-handed open rings, recently resolved by cryo-EM (22) (Fig. 8, *A* and *B*). The assembly of these oligomers likely coincides with multiple AAA subunits binding the C-terminal β -tubulin tails, which are exposed on the MT surface (30). The formation of these spirals is likely slow and requires the effect of MT and ATP binding to each subunit to form assemblies. In the studies by Zehr *et al.* (22), these were stabilized by blocking ATP hydrolysis with the Glu \rightarrow Gln

mutant. However, previous FRET experiments suggested that this monomer to oligomer transition requires both ATP binding and MT binding (19). *In vivo* assembly of right-handed open rings might be promoted or activated by regulators such as ASPM (2) or patronin/CAMSAP (29), which bind the MIT/con80 complex and recruit them to MTs. Initially, the open right-handed spiral of ATP-bound protomers would thread the β -tubulin C-terminal domain into its pore through the \sim 40-Å gap in the ring. As suggested previously by Zehr *et al.* (22), upon hydrolysis of the ATP bound to three adjacent protomers and release of nucleotide from one protomer, the right-handed spiral would close into a flat ring encircling the β -tubulin tail (Fig.

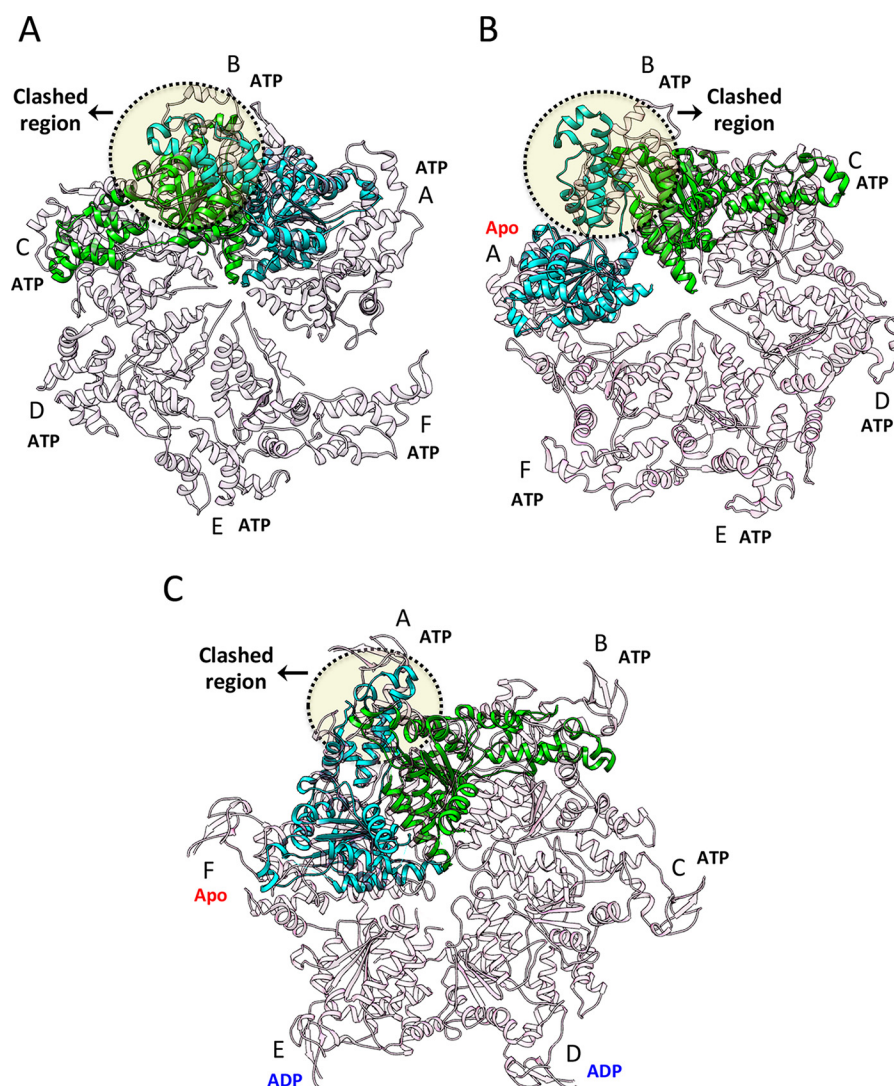


Figure 5. Comparisons of nucleotide-free katanin structure with hexameric assemblies of MEI-1 EQ AAA and Vps4 structures reveal nucleotide-free katanin structure in an autoinhibited state. Superimpositions are shown of nucleotide-free KATNAL1 (E308Q) AAA structures (cyan and green) onto two adjacent protomers in an ATP-bound MEI-1 right-handed ring (A), a MEI-1 closed-ring (B), and Vps4 hexameric ring (C) with the backbones shown as ribbon diagrams (light pink), respectively. Note that the clashed regions in all panels (highlighted by dotted-line yellow background circle) show that the conformation of KATNAL1 (E308Q) AAA is incompatible with hexameric assemblies, confirming that the KATNAL1 (E308Q) AAA structure is in an autoinhibited state.

Table 3
RMSD values of various AAA katanin orthologs

Protein	Source	Nucleotide	PDB ID	RMSD ^a
MEI-1 AAA	<i>C. elegans</i>	ADP	Present study	1.50
MEI-1 AAA (E293Q)	<i>C. elegans</i>	Apo	5WCB, chain A	2.92
MEI-1 AAA (E293Q)	<i>C. elegans</i>	ATP	5WC0, chain B	2.43
VPS4 ^b	<i>Saccharomyces cerevisiae</i>	ADP	5UIE, chain E	1.83
VPS4 ^b	<i>S. cerevisiae</i>	ADP-BeF ₄	5UIE, chain A	2.36
VPS4 ^b	<i>S. cerevisiae</i>	Apo	5UIE, chain F	1.38
VPS4 ^b	<i>Metallophaera sedula</i>	ADP	4D81	1.41
VPS4 ^b	<i>M. sedula</i>	Apo	4D80, chain A	1.31
Spastin	<i>Drosophila melanogaster</i>	Apo	3B9P	1.41
Spastin	<i>Homo sapiens</i>	Apo	3VFD	1.61
Fidgetin	<i>C. elegans</i>	Apo	4L15	1.86
Fidgetin	<i>C. elegans</i>	ADP	4L16	1.81

^a The structure is superimposed onto the NBD domain (residues 207–378, C α positions) of KATNAL1 AAA ATPase with a RMSD.

^b Vacuolar protein sorting–associated protein 4.

8C). This transition is similar to that proposed for VPS4 (25, 28, 31, 32) and is supported by a flat ring structure of MEI-1 as determined by cryo-EM (22). However, upon hydrolysis of the

ATPs associated with the remaining three protomers, we suggest that the flat hexameric ring would transition to the left-handed spiral conformation (Fig. 8D) with five ADP protomers and one nucleotide-free protomer. In contrast to the conclusions drawn by Zehr *et al.* (22), we suggest that katanin transitions from a closed hexamer to a left-handed spiral after ATP hydrolysis and phosphate release (Fig. S8). In this left-handed spiral state, the NBD pore loops are repositioned further away from the microtubule surface, leading to a pulling effect on the β -tubulin C terminus away from the MT surface. This flat ring to spiral conformational change likely induces the removal of an $\alpha\beta$ -tubulin dimer from the MT lattice. The dissociation of ADP would result in katanin oligomers rapidly disassembling to the monomeric nucleotide-free state (Fig. 8A). Our model suggests that hexameric assembly is transient followed by one or a few tubulin removal cycles and then by rapid disassembly of katanin. Our model suggests that the hexamers rapidly disassemble and are likely not processive enzymes.

Katanin nucleotide-free state reveals disassembly mechanism

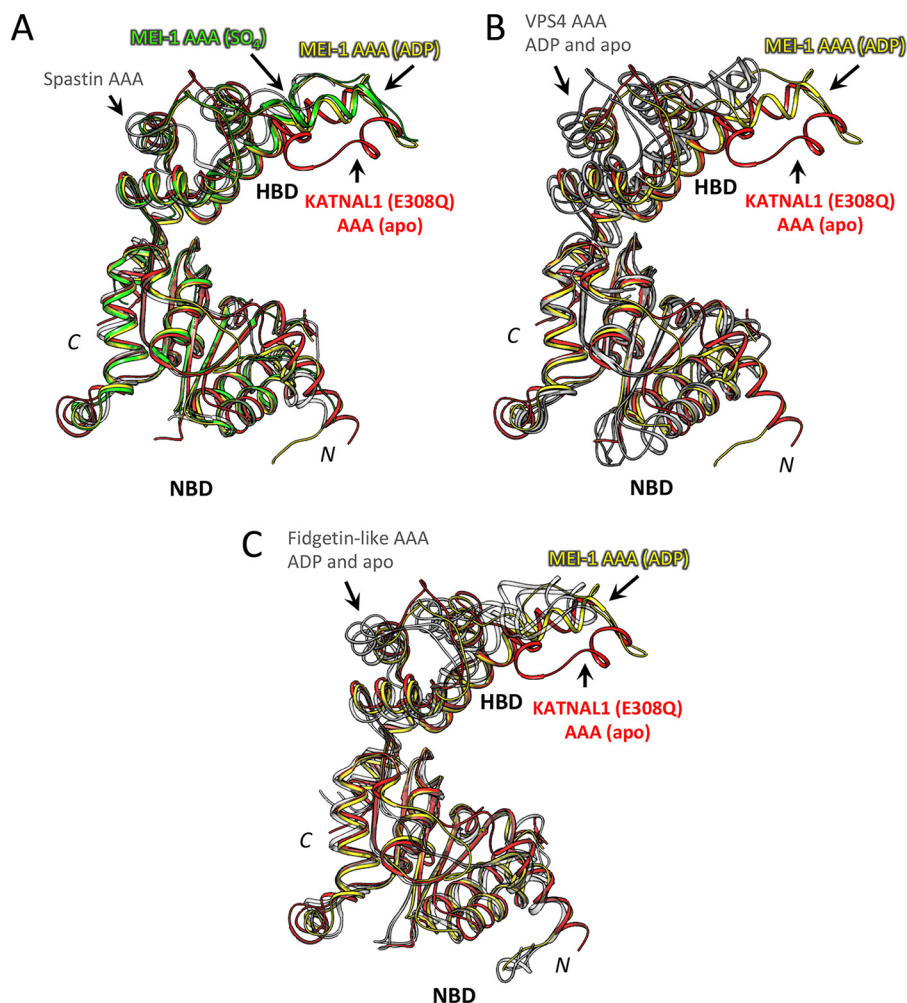


Figure 6. Comparisons of katanin structures with other AAA ATPase modules. *A*, superimposition of the KATNAL1 (E308Q) AAA structure (red) onto the ADP state of MEI-1 AAA (yellow), sulfate-bound MEI-1 AAA (green, PDB code 5WC1), and spastin (dark gray, PDB code 3B9P); *B*, onto different states of Vps4 (gray, PDB code 4D81, ADP state; PDB code 4D80, chain A, nucleotide-free or apo-state); and *C*, different states of fidgetin-like AAA (gray, PDB code 4L16, ADP state; and PDB code 4L15, nucleotide-free or apo-state) structures, respectively. Comparisons of these structures reveal that KATNAL1 (E308Q) AAA structure is in a different conformation. The RMSD values of these structures are given in Table 3.

Zehr *et al.* (22) suggest that the right-handed open ring to closed hexameric ring structure transition constitutes the power stroke for pulling a β -tubulin tail from the MT lattice. This transition, however, generates a ~ 20 -Å displacement between pore loops and collectively through sequential cycles of ATP hydrolysis, resulting in the β -tubulin C terminus being translocated 120 Å perpendicular to the MT surface. In contrast, the ADP-bound katanin AAA structure proposed in our model indicates that the transition from a right-handed spiral to a left-handed spiral will likely mobilize the pore loops more than three times this distance (~ 60 -Å) in a single event, without processive ATP hydrolysis steps around the AAA hexameric ring. We suggest that the larger displacement followed by rapid dissociation to a self-inhibited monomeric state more likely explains how the tubulin dimer is pulled from the lattice by this dynamic AAA enzyme.

Experimental procedures

Protein expression and purification of katanin complexes

The coding regions for katanin p60 from human KATNAL1 (accession number Q9BW62.1), and *C. elegans* MEI-1 (acces-

sion number AAA28109.1) were inserted into bacterial expression vectors (pCDF-Duet-TEV) with no tag using isothermal assembly. The human KATNAL1 inactive mutant (E308Q) was generated and inserted into a bacterial expression vector (V2-H6-GST-TEV) with a His tag, a GST tag, and a TEV cleavage site. The coding regions for con-80 from *C. elegans* MEI-2 (accession number AAF62184.1) and human KATNB1 (accession number CAG33043.1) were inserted into bacterial expression vectors (pMAL-CRI-TEV vector) with an MBP (maltose-binding protein) tag and a TEV cleavage site using isothermal assembly. These constructs were confirmed by DNA sequencing.

Recombinant WT KATNAL1/B1-con80 and MEI-1/MEI-2 complexes were purified as follows. Constructs were co-transformed and expressed in BL21 bacterial strains using the T7 expression system, grown at 37 °C, and induced with 0.5 mM isopropyl thio- β -glycoside at 18 °C overnight. Cells were centrifuged and resuspended in 40 mM HEPES, pH 7.3, 300 mM NaCl, 2 mM MgCl₂, and 3 mM β -mercaptoethanol (KATN buffer). Cells were lysed using a Microfluidizer (Avastin). Extracts were clarified via centrifugation at 18,000 \times g. Pro-

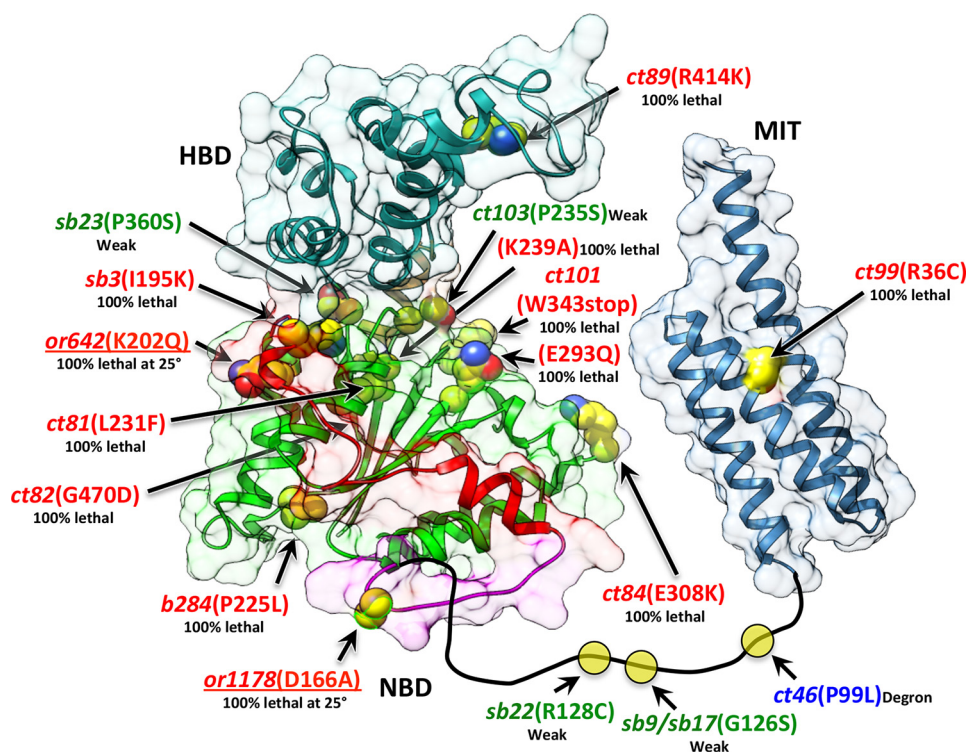


Figure 7. Mapping the *mei-1* *C. elegans* meiosis mutations onto structural full-length MEI-1 p60 model. MEI-1 AAA (color-coded according to the structure) and MIT (blue) are shown in ribbon representations with a molecular transparent surface background; mutated residues are shown as yellow spheres with heteroatom colors. Phenotypes of functional mutations are labeled in different colors (100% lethal and no spindle poles, red; 100% lethal at 25 °C, red and underlined; weak and partial loss of function, green; and degron, blue). The MIT domain was modeled based on the *M. musculus* MIT structure (2).

teins were purified and cleaved with TEV protease while attached to the amylose resin (New England Biolabs). Proteins were further purified by ion exchange using Hitrap-SP chromatography followed by size-exclusion chromatography using a Superose 6 (10/300) column (GE Healthcare). The proteins were then used in subsequent studies as described below without freezing.

Recombinant KATNAL1 (E308Q)/B1-con80 protein was expressed in bacteria using the approach described above. The protein was purified and cleaved with TEV protease while it was attached to the amylose resin. Cleaved GST and impurities were removed by nickel-nitrilotriacetic acid, GST resin, and ion exchange using Hitrap-SP chromatography. The protein was further purified using a Superose 6 (10/300) gel filtration column. The final protein was then used in subsequent studies without freezing.

Selenomethionine-substituted (Se-MEI-1/MEI-2) katanin complex was expressed in BL21 *Escherichia coli* strain using a metabolic labeling strategy, where growth and expression were performed using minimal media containing all amino acids but with selenomethionine replacing Met (33). The complex was purified using the strategy described above. 1 mM DTT was used throughout the purification steps.

Biochemical analyses of oligomeric katanin assemblies

To assess the oligomeric assemblies of the KATNAL1/B1-con80 and MEI-1/MEI-2 complexes, size-exclusion chromatography was performed at 4 °C. A Superose 6 size-exclusion column or Superdex 200 (SEC) was calibrated with molecular mass standards (Bio-Rad). The protein samples were analyzed

at concentrations ranging from 5 to 50 μ M by mixing the complex with or without 1 mM ATP into 0.5-ml volumes and injected them into a SEC column equilibrated in KATN buffer supplemented with 1 mM ATP using an AKTA purifier system (GE Healthcare). Elution fractions (0.5 ml) were collected and analyzed via SDS-PAGE. The molar ratios for KATNAL1 or KATNAL1 (E308Q) to KATNB1-con80 and MEI-1 to MEI-2 were quantitated using densitometry. Molecular masses of various concentrations of KATNAL1/B1-con80 and/or MEI-1/MEI-2 complexes supplemented with or without 1 mM ATP were measured using SEC-MALS with KATN buffer at 25 °C. The complexes were analyzed on Superdex 200 SEC column (GE Healthcare) along with UV spectrophotometer (Agilent 1100-Series HPLC), light scattering (Wyatt Technology: miniDAWN TREOS), and the refractive index (Wyatt Technology: Optilab T-rEX). Concentration-weighted molecular masses for each peak were calculated using ASTRA v. 6 software (Wyatt Technology). The SEC-MALS fractions were collected manually for one of the concentrations (25 μ M), and the compositions were checked using SDS-PAGE, confirming that complexes were intact (Fig. S2C). The remaining concentrations were performed using a Superdex 200 column at 4 °C in the presence or absence of 1 mM ATP with WT KATNAL1/B1-Con80 or E308Q mutant of KATNAL1/B1-con80, and the compositions were confirmed by SDS-PAGE (Fig. S2, A and B).

Crystallization of katanin in the ADP-bound and monomeric states

Katanin complexes (KATNAL1 (E308Q)/B1-con80 and MEI-1/MEI-2) were screened for crystallization with a com-

Katanin nucleotide-free state reveals disassembly mechanism

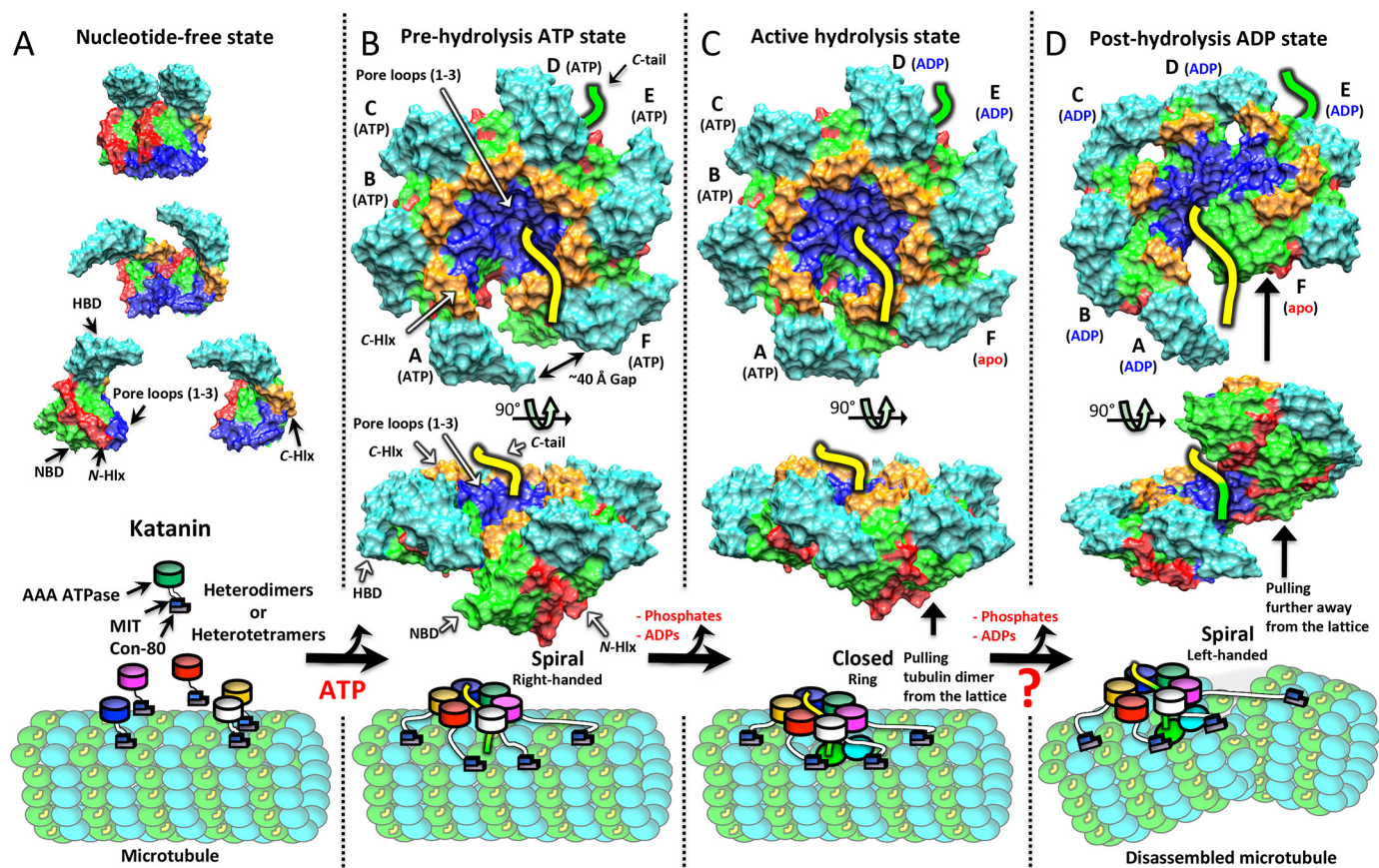


Figure 8. Structural model for katanin AAA microtubule-based assembly and severing. *A*, upper panel, katanin AAA ATPase in nucleotide-free state, which forms self-inhibited monomers or dimers in solution (see Fig. 2). N-Hlx, red; NBD, light green; HBD, cyan; C-Hlx, orange; and pore loops 1–3, blue. Lower panel, cartoon diagrams of katanin p60/p80 (con80 domain) complexes diffusing on the MT lattice (α -tubulin, cyan; β -tubulin, light green; and C-terminal tail or C-tail of β -subunit, yellow) in the absence of nucleotide. MIT (blue), con80 (light purple), and AAA (green, magenta, blue, white, and gold) domains are shown. *B*, upper panel, side view of hexameric right-handed spiral model (produced based on MEI-1 right-handed spiral assembly as described in Fig. S7) of katanin AAA ATPase in prehydrolysis ATP state. Note that the pore loops engage the β -tubulin C-terminal tail (yellow) emanating from the MT lattice surface. Middle panel, perpendicular view of the same assembly. Lower panel, schematic diagram of heterododecameric p60/p80 right-handed spiral katanin complex binding onto MT lattice via C-tail in the presence of ATP. *C*, upper panel, side view of closed ring model (produced based on Vps4, described in Fig. S7) of katanin AAA ATPase in an active hydrolysis state. Middle panel, perpendicular view of the same model. Lower panel, ring structure of heterododecameric katanin complex displacing the tubulin dimer through C-tail from the MT lattice. *D*, upper panel, side view of hexameric left-handed spiral model of katanin AAA ATPase in post-hydrolysis ADP state (see Fig. 2). Middle panel, perpendicular view of the same model. Lower panel, cartoon representation of heterododecameric left-handed spiral katanin complex pulling the tubulin dimer farther away from the lattice, which leads to the formation of two new MTs.

mercial sparse matrix (Qiagen, Valencia, CA) or homemade screens in a 96-well format using a Mosquito robot (TTP Labtech, Oxford, UK) via the hanging-drop method and a protein concentration of 10 mg/ml supplemented with 1 mM AMP-PNP at 293 K. ADP-bound selenomethionine-substituted protein crystals grew over 7–15 days in a reservoir solution of 0.1 M HEPES, pH 7.0, and 1.0 M sodium potassium tartrate. Larger cylinder-shaped crystals were formed 2 weeks after microseeding in 0.1 M HEPES, pH 7.5, and 0.7 M sodium potassium tartrate. Nucleotide-free rectangular crystals were obtained and refined using 0.1 M Tris, pH 8.0, and 18% PEG 8000. Rectangular crystals appeared in 1 week and grew to maximal size in 2 weeks. To obtain phase information, native nucleotide-free crystals were soaked in mother liquor containing potassium tetrabromoaurate(III) dehydrate (Hampton Research) and transferred to cryoprotectant condition.

X-ray data collection and structure determination

For cryoprotection, ADP-bound and nucleotide-free crystals were soaked for 30–60 s in corresponding reservoir solutions

supplemented with 30% (v/v) glycerol or 30% (v/v) PEG 400. Crystals were mounted in a cryo-loop (Hampton Research) and then immediately flash-cooled in liquid nitrogen. Diffraction data, collected at the Argonne National Laboratory at the Advanced Photon Source microfocus 24-ID-C or 24-ID-E beamline, were processed with XDS (34) or iMosfilm (35) and Scala (36).

The ADP-bound cylinder-shaped crystals were obtained from MEI-1/MEI-2 complex, and one of the best crystals was diffracted to 3.1-Å resolution in a hexagonal ($P6_3$) space group with cell dimensions $a = 98.83$, $b = 98.83$, and $c = 75.08$ Å. The structure was determined using phases obtained from a SAD dataset from crystals grown from selenomethionine-derivatized protein. Automated XDS→SHELX→PHENIX for the SAD dataset was performed by the RAPD data processing pipeline at the Synchrotron NE-CAT beamline (<https://rapd.nec.aps.anl.gov>). Selenium sites identified using the SHELX suite (37) were refined to a 0.65 figure of merit and then supplied to an AutoBuild module using the program RESOLVE in the PHENIX program suite (38). Automatic chain tracing

yielded several helical fragments. Manual tracing in the program COOT was used to fill the gaps (39). The density map indicated a MEI-1 AAA domain in the asymmetric unit. The N-terminal MIT domain and MEI-2 could not be identified in the density map, revealing that it underwent proteolysis during crystallization. A Matthews coefficient calculation of the solvent content supports the idea that only the MEI-1 AAA domain is contained in the crystal (40). The final model was refined using PHENIX program and torsion-angle molecular dynamics with a slow-cooling simulated annealing and TLS (Translation/Libration/Screw) schemes to $R_{\text{free}}/R_{\text{work}}$ (0.26/0.21). The MEI-1 AAA structure consists of residues 164–265, 270–298, 308–325, and 331–468 and an ADP molecule. Despite the presence of the nonhydrolyzable analogue AMP-PNP in the crystallization condition, only ADP was identified at the active site, suggesting that AMP-PNP underwent hydrolysis during crystallization. Data processing and refinement statistics are given in Table 2.

The best nucleotide-free rectangular crystals formed from KATNAL1 (E308Q)/B1-con80 complex crystals and diffracted to 2.4 Å. Diffraction data were collected for the best nucleotide-free rectangular crystals obtained from KATNAL1 (E308Q)/B1-con80 complex in the $P2_12_12_1$ space group to 2.4 Å resolution with unit cell dimensions $a = 40.10$, $b = 61.19$, and $c = 117.62$ Å. Phase information was determined by molecular replacement using the NBD domain (polyalanine model) of MEI-1 AAA as the search model. An unambiguous rotation and translation solution was obtained using the program PHASER (41). Gold substructures were obtained by running PHASER in its MR-SAD mode with phases from NBD polyalanine model. This phase was subjected to density modification with solvent flattening and histogram matching as implemented in the CCP4 suite (42). Automatic chain tracing using RESOLVE yielded several helical fragments of the HBD domain. Manual tracing in the program COOT was used to fill the gaps (39). The asymmetric unit contains only a KATNAL1 (E308Q) AAA domain; the N-terminal MIT domain and KATNB1 could not be identified, suggesting that these domains underwent proteolysis during crystallization and were likely lost. A Matthews coefficient calculation also supports the hypothesis that only the KATNAL1 (E308Q) AAA domain is contained in the crystal (40). The final model was refined using the PHENIX program (43) and torsion-angle molecular dynamics with a slow-cooling simulated annealing and TLS schemes to $R_{\text{free}}/R_{\text{work}}$ (0.25/0.22). The KATNAL1 (E308Q) AAA structure consists of residues 184–280, 285–315, 318–339, and 348–490, tetraethylene glycol, and 53 water molecules. No nucleotide was identified in the density map, despite the presence of the nonhydrolyzable analogue AMP-PNP in the crystallization condition.

The stereochemical properties of the final models, KATNAL1 (E308Q) AAA and MEI-1 AAA, were assessed using the program MolProbity (44). All structure-rendering figures were generated using UCSF Chimera (45) and PyMOL (48).

Molecular modeling of N-terminal MIT domain and hexameric katanin assemblies

Two different monomeric states (ATP and ADP states) of the AAA domain from the human KATNAL1 sequence (residues

184–490) were built by homology templates to the cryo-EM structure of the MEI-1 AAA hexameric right-handed spiral (PDB code 5WC0, ATP state, chain B (22)) and current ADP-bound MEI-1 AAA (PDB code 5B5D) structure, respectively (Fig. S7, A and B). To build a prehydrolysis ATP-state model (Fig. S7C), C α atoms of the monomeric AAA-ATP-state models were optimally superposed to two adjacent protomers in the cryo-EM structure of the MEI-1 AAA hexameric right-handed spiral (22). This process was repeated up to a desired number of times to construct hexameric right-handed spiral assembly. The same approach was applied to get the katanin active-state model by different nucleotide states of AAA protomers (monomeric models and autoinhibited nucleotide-free structures) onto the six AAA modules of the VPS4 hexameric closed-ring structure (Fig. S7D) (25). The post-hydrolysis state model of human katanin was generated by different nucleotides states of AAA protomers (ADP state and autoinhibited nucleotide-free structures) onto the six AAA modules of the current MEI-1 AAA pseudo-hexameric left-handed spiral assembly (Fig. S7E). These models were energy minimized using the program CNS (46).

To generate a structural model of full MEI-1 P60 for mapping *C. elegans* mei1 meiosis mutations, a model of the N-terminal MIT domain of *C. elegans* was built by homology to the crystal structure of the MIT domain of the *M. musculus* p60N/p80C katanin complex (PDB code 5NBT (2)). The MIT domain model was generated using UCSF Chimera (45) and Modeler (47) followed by energy minimization with the CNS program (46).

Author contributions—S. N., F. J. M., and J. A.-B. conceptualization; S. N. software; S. N. and J. A.-B. validation; S. N. and J. A.-B. investigation; S. N. and J. A.-B. visualization; S. N. methodology; S. N., F. J. M., and J. A.-B. writing-original draft; S. N., F. J. M., and J. A.-B. writing-review and editing; J. A.-B. data curation; J. A.-B. supervision; J. A.-B. project administration.

Acknowledgments—We thank Advanced Photon Source and Drs. K. Rajashankar, J. Schuermann, and D. Neau of the Northeastern Collaborative Access Team (NE-CAT) for the use of the 24-IDC and IDE beam lines to collect all the X-ray diffraction data for our crystallographic studies. We thank our graduate student, Brian D. Cook, for help with SEC-MALS. This work is based upon research conducted at the NE-CAT beamlines, which are funded by the National Institute of General Medical Sciences from the National Institutes of Health (P41 GM103403). The Pilatus 6M detector on 24-ID-C beam line is funded by a NIH-ORIP HEI grant (S10 RR029205). The Eiger 16M detector on 24-ID-E beam line is funded by a NIH-ORIP HEI grant (S10OD021527). This research used resources of the Advanced Photon Source, a U.S. Department of Energy (DOE) Office of Science User Facility operated for the DOE Office of Science by Argonne National Laboratory under Contract No. DE-AC02-06CH11357.

References

1. Roll-Mecak, A., and McNally, F. J. (2010) Microtubule-severing enzymes. *Curr. Opin. Cell Biol.* **22**, 96–103 [CrossRef Medline](#)
2. Jiang, K., Rezabkova, L., Hua, S., Liu, Q., Capitani, G., Altelaar, A. F. M., Heck, A. J. R., Kammerer, R. A., Steinmetz, M. O., and Akhmanova, A. (2017) Microtubule minus-end regulation at spindle poles by an ASPM-katanin complex. *Nat. Cell Biol.* **19**, 480–492 [CrossRef Medline](#)

Katanin nucleotide-free state reveals disassembly mechanism

- McNally, K., Audhya, A., Oegema, K., and McNally, F. J. (2006) Katanin controls mitotic and meiotic spindle length. *J. Cell Biol.* **175**, 881–891 [CrossRef Medline](#)
- Ahmad, F. J., Yu, W., McNally, F. J., and Baas, P. W. (1999) An essential role for katanin in severing microtubules in the neuron. *J. Cell Biol.* **145**, 305–315 [CrossRef Medline](#)
- Sharma, N., Bryant, J., Wloga, D., Donaldson, R., Davis, R. C., Jerka-Dziadosz, M., and Gaertig, J. (2007) Katanin regulates dynamics of microtubules and biogenesis of motile cilia. *J. Cell Biol.* **178**, 1065–1079 [CrossRef Medline](#)
- Mishra-Gorur, K., Çalayan, A. O., Schaffer, A. E., Chabu, C., Henegariu, O., Vonhoff, F., Akgümü, G. T., Nishimura, S., Han, W., Tu, S., Baran, B., Gümü, H., Dilber, C., Zaki, M. S., Hossni, H. A., *et al.* (2014) Mutations in KATNB1 cause complex cerebral malformations by disrupting asymmetrically dividing neural progenitors. *Neuron* **84**, 1226–1239 [CrossRef Medline](#)
- Hu, W. F., Pomp, O., Ben-Omran, T., Kodani, A., Henke, K., Mochida, G. H., Yu, T. W., Woodworth, M. B., Bonnard, C., Raj, G. S., Tan, T. T., Hamamy, H., Masri, A., Shboul, M., Al Saffar, M., *et al.* (2014) Katanin p80 regulates human cortical development by limiting centriole and cilia number. *Neuron* **84**, 1240–1257 [CrossRef Medline](#)
- Hazan, J., Fonknechten, N., Mavel, D., Paternotte, C., Samson, D., Artiguenave, F., Davoine, C. S., Cruaud, C., Dürr, A., Wincker, P., Brottier, P., Cattolico, L., Barbe, V., Burgunder, J. M., Prud'homme, J. F., *et al.* (1999) Spastin, a new AAA protein, is altered in the most frequent form of autosomal dominant spastic paraplegia. *Nat. Genet.* **23**, 296–303 [CrossRef Medline](#)
- McNally, F. J., and Vale, R. D. (1993) Identification of katanin, an ATPase that severs and disassembles stable microtubules. *Cell* **75**, 419–429 [CrossRef Medline](#)
- Iwaya, N., Kuwahara, Y., Fujiwara, Y., Goda, N., Tenno, T., Akiyama, K., Mase, S., Tochio, H., Ikegami, T., Shirakawa, M., and Hiroaki, H. (2010) A common substrate recognition mode conserved between katanin p60 and VPS4 governs microtubule severing and membrane skeleton reorganization. *J. Biol. Chem.* **285**, 16822–16829 [CrossRef Medline](#)
- McNally, F. J., and Thomas, S. (1998) Katanin is responsible for the M-phase microtubule-severing activity in *Xenopus* eggs. *Mol. Biol. Cell* **9**, 1847–1861 [CrossRef Medline](#)
- Srayko, M., Buster, D. W., Bazirgan, O. A., McNally, F. J., and Mains, P. E. (2000) MEI-1/MEI-2 katanin-like microtubule severing activity is required for *Caenorhabditis elegans* meiosis. *Genes Dev.* **14**, 1072–1084 [CrossRef Medline](#)
- Fleming, K. G., Hohl, T. M., Yu, R. C., Müller, S. A., Wolpensinger, B., Engel, A., Engelhardt, H., Brünger, A. T., Söllner, T. H., and Hanson, P. I. (1998) A revised model for the oligomeric state of the *N*-ethylmaleimide-sensitive fusion protein, NSF. *J. Biol. Chem.* **273**, 15675–15681 [CrossRef Medline](#)
- DeLaBarre, B., and Brunger, A. T. (2005) Nucleotide dependent motion and mechanism of action of p97/VCP. *J. Mol. Biol.* **347**, 437–452 [CrossRef Medline](#)
- Fletcher, R. J., Bishop, B. E., Leon, R. P., Sclafani, R. A., Ogata, C. M., and Chen, X. S. (2003) The structure and function of MCM from archaeal *thermoautotrophicum*. *Nat. Struct. Biol.* **10**, 160–167 [CrossRef Medline](#)
- Suno, R., Niwa, H., Tsuchiya, D., Zhang, X., Yoshida, M., and Morikawa, K. (2006) Structure of the whole cytosolic region of ATP-dependent protease FtsH. *Mol. Cell* **22**, 575–585 [CrossRef Medline](#)
- Wohlever, M. L., Mateja, A., McGilvray, P. T., Day, K. J., and Keenan, R. J. (2017) Msp1 is a membrane protein dislocase for tail-anchored proteins. *Mol. Cell* **67**, 194–202 [CrossRef Medline](#)
- Roll-Mecak, A., and Vale, R. D. (2008) Structural basis of microtubule severing by the hereditary spastic paraplegia protein spastin. *Nature* **451**, 363–367 [CrossRef Medline](#)
- Hartman, J. J., and Vale, R. D. (1999) Microtubule disassembly by ATP-dependent oligomerization of the AAA enzyme katanin. *Science* **286**, 782–785 [CrossRef Medline](#)
- Babst, M., Wendland, B., Estepa, E. J., and Emr, S. D. (1998) The Vps4p AAA ATPase regulates membrane association of a Vps protein complex required for normal endosome function. *EMBO J.* **17**, 2982–2993 [CrossRef Medline](#)
- Scott, A., Chung, H. Y., Gonciarz-Swiatek, M., Hill, G. C., Whitby, F. G., Gaspar, J., Holton, J. M., Viswanathan, R., Ghaffarian, S., Hill, C. P., and Sundquist, W. I. (2005) Structural and mechanistic studies of VPS4 proteins. *EMBO J.* **24**, 3658–3669 [CrossRef Medline](#)
- Zehr, E., Szyk, A., Piszczek, G., Szczesna, E., Zuo, X., and Roll-Mecak, A. (2017) Katanin spiral and ring structures shed light on power stroke for microtubule severing. *Nat. Struct. Mol. Biol.* **24**, 717–725 [CrossRef Medline](#)
- Joly, N., Martino, L., Gigant, E., Dumont, J., and Pintard, L. (2016) Microtubule-severing activity of the AAA+ ATPase katanin is essential for female meiotic spindle assembly. *Development* **143**, 3604–3614 [CrossRef Medline](#)
- Taylor, J. L., White, S. R., Lauring, B., and Kull, F. J. (2012) Crystal structure of the human spastin AAA domain. *J. Struct. Biol.* **179**, 133–137 [CrossRef Medline](#)
- Monroe, N., Han, H., Shen, P. S., Sundquist, W. I., and Hill, C. P. (2017) Structural basis of protein translocation by the Vps4-Vta1 AAA ATPase. *Elife* **6**, e24487 [CrossRef Medline](#)
- Clark-Maguire, S., and Mains, P. E. (1994) Localization of the mei-1 Gene product of *Caenorhabditis elegans*, a meiotic-specific spindle component. *J. Cell Biol.* **126**, 11 [CrossRef](#)
- Hartman, J. J., Mahr, J., McNally, K., Okawa, K., Iwamoto, A., Thomas, S., Cheesman, S., Heuser, J., Vale, R. D., and McNally, F. J. (1998) Katanin, a microtubule-severing protein, is a novel AAA ATPase that targets to the centrosome using a WD40-containing subunit. *Cell* **93**, 277–287 [CrossRef Medline](#)
- Han, H., Monroe, N., Sundquist, W. I., Shen, P. S., and Hill, C. P. (2017) The AAA ATPase Vps4 binds ESCRT-III substrates through a repeating array of dipeptide-binding pockets. *Elife* **6**, e31324 [CrossRef Medline](#)
- Jiang, K., Hua, S., Mohan, R., Grigoriev, I., Yau, K. W., Liu, Q., Katrukha, E. A., Altelaar, A. F., Heck, A. J., Hoogenraad, C. C., and Akhmanova, A. (2014) Microtubule minus-end stabilization by polymerization-driven CAMSAP deposition. *Dev. Cell* **28**, 295–309 [CrossRef Medline](#)
- Bailey, M. E., Sackett, D. L., and Ross, J. L. (2015) Katanin severing and binding microtubules are inhibited by tubulin carboxy tails. *Biophys. J.* **109**, 2546–2561 [CrossRef Medline](#)
- Sun, S., Li, L., Yang, F., Wang, X., Fan, F., Yang, M., Chen, C., Li, X., Wang, H. W., and Sui, S. F. (2017) Cryo-EM structures of the ATP-bound Vps4E233Q hexamer and its complex with Vta1 at near-atomic resolution. *Nat. Commun.* **8**, 16064 [CrossRef Medline](#)
- Su, M., Guo, E. Z., Ding, X., Li, Y., Tarrasch, J. T., Brooks, C. L., 3rd, Xu, Z., and Skiniotis, G. (2017) Mechanism of Vps4 hexamer function revealed by cryo-EM. *Sci. Adv.* **3**, e1700325 [CrossRef Medline](#)
- Van Duyne, G. D., Standaert, R. F., Karplus, P. A., Schreiber, S. L., and Clardy, J. (1993) Atomic structures of the human immunophilin FKBP-12 complexes with FK506 and rapamycin. *J. Mol. Biol.* **229**, 105–124 [CrossRef Medline](#)
- Kabsch, W. (2010) XDS. *Acta Crystallogr. D Biol. Crystallogr.* **66**, 125–132 [CrossRef Medline](#)
- Powell, H. R., Johnson, O., and Leslie, A. G. (2013) Autoindexing diffraction images with iMosflm. *Acta Crystallogr. D Biol. Crystallogr.* **69**, 1195–1203 [CrossRef Medline](#)
- Evans, P. (2006) Scaling and assessment of data quality. *Acta Crystallogr. D Biol. Crystallogr.* **62**, 72–82 [CrossRef Medline](#)
- Sheldrick, G. M. (2010) Experimental phasing with SHELXC/D/E: Combining chain tracing with density modification. *Acta Crystallogr. D Biol. Crystallogr.* **66**, 479–485 [CrossRef Medline](#)
- Terwilliger, T. C., Adams, P. D., Read, R. J., McCoy, A. J., Moriarty, N. W., Grosse-Kunstleve, R. W., Afonine, P. V., Zwart, P. H., and Hung, L. W. (2009) Decision-making in structure solution using Bayesian estimates of map quality: The PHENIX AutoSol wizard. *Acta Crystallogr. D Biol. Crystallogr.* **65**, 582–601 [CrossRef Medline](#)
- Emsley, P., and Cowtan, K. (2004) Coot: Model-building tools for molecular graphics. *Acta Crystallogr. D Biol. Crystallogr.* **60**, 2126–2132 [CrossRef Medline](#)
- Matthews, B. W. (1968) Solvent content of protein crystals. *J. Mol. Biol.* **33**, 491–497 [CrossRef Medline](#)

41. McCoy, A. J., Grosse-Kunstleve, R. W., Adams, P. D., Winn, M. D., Storoni, L. C., and Read, R. J. (2007) Phaser crystallographic software. *J. Appl. Crystallogr.* **40**, 658–674 [CrossRef Medline](#)
42. Potterton, E., Briggs, P., Turkenburg, M., and Dodson, E. (2003) A graphical user interface to the CCP4 program suite. *Acta Crystallogr. D Biol. Crystallogr.* **59**, 1131–1137 [CrossRef Medline](#)
43. Adams, P. D., Grosse-Kunstleve, R. W., Hung, L. W., Ioerger, T. R., McCoy, A. J., Moriarty, N. W., Read, R. J., Sacchettini, J. C., Sauter, N. K., and Terwilliger, T. C. (2002) PHENIX: Building new software for automated crystallographic structure determination. *Acta Crystallogr. D Biol. Crystallogr.* **58**, 1948–1954 [CrossRef Medline](#)
44. Chen, V. B., Arendall, W. B., 3rd, Headd, J. J., Keedy, D. A., Immormino, R. M., Kapral, G. J., Murray, L. W., Richardson, J. S., and Richardson, D. C. (2010) MolProbity: All-atom structure validation for macromolecular crystallography. *Acta Crystallogr. D Biol. Crystallogr.* **66**, 12–21 [CrossRef Medline](#)
45. Pettersen, E. F., Goddard, T. D., Huang, C. C., Couch, G. S., Greenblatt, D. M., Meng, E. C., and Ferrin, T. E. (2004) UCSF Chimera: A visualization system for exploratory research and analysis. *J. Comput. Chem.* **25**, 1605–1612 [CrossRef Medline](#)
46. Brunger, A. T. (2007) Version 1.2 of the crystallography and NMR system. *Nat. Protoc.* **2**, 2728–2733 [CrossRef Medline](#)
47. Sali, A., and Blundell, T. L. (1993) Comparative protein modelling by satisfaction of spatial restraints. *J. Mol. Biol.* **234**, 779–815 [CrossRef Medline](#)
48. DeLano, W. L. (2012) *The PyMOL Molecular Graphics System*, version 1.5.0.1, Schroedinger, LLC, New York

Structural basis for disassembly of katanin heterododecamers
Stanley Nithianantham, Francis J. McNally and Jawdat Al-Bassam

J. Biol. Chem. 2018, 293:10590-10605.

doi: 10.1074/jbc.RA117.001215 originally published online May 11, 2018

Access the most updated version of this article at doi: [10.1074/jbc.RA117.001215](https://doi.org/10.1074/jbc.RA117.001215)

Alerts:

- [When this article is cited](#)
- [When a correction for this article is posted](#)

[Click here](#) to choose from all of JBC's e-mail alerts

This article cites 47 references, 13 of which can be accessed free at <http://www.jbc.org/content/293/27/10590.full.html#ref-list-1>